Supplementary Information (SI)

High-performance carbon fibers fabricated from coal and waste plastics

Zhe Chen,[a] Wenjia Wang,[b] Tongtong Wang,[c] Sean Tang,[a] Sabin Gautam,[d] Nilay Saha,[e] Piumi Samarawickrama,[d] So Tie Tjeng,[c] Eric Eddings*[b] and Maohong Fan*[fg]

[a] *Department of Energy & Petroleum Engineering, University of Wyoming, Laramie, WY 82071, USA*

[b] *Department of Chemical Engineering, University of Utah, Salt Lake City, UT 84112, USA*

[c] *Department of Chemical and Biomedical Engineering, University of Wyoming, Laramie, WY 82071, USA*

[d] *Department of Physics and Astronomy, University of Wyoming, Laramie, WY 82071, USA*

[e] *Department of Chemistry, University of Wyoming, Laramie, WY 82071, USA*

[f] *College of Engineering and Physical Sciences, and School of Energy Resources, University of Wyoming, Laramie, WY 82071, USA.*

[g] *College of Engineering, Georgia Institute of Technology, Atlanta, GA 30332, USA*

Dr. Maohong Fan: mfan@uwyo.edu, Dr. Eric Eddings: eric.eddings@chemeng.utah.edu

1 HDPE hydrogenolysis

Hydrogenolysis of HDPE was performed to acquire plastic-derived liquid (PDL). HDPE was purchased from Sigma Aldrich. 50 g HDPE was loaded into a Parr 4571 batch reactor whose vessel had capacity of 1.0 L. The reactor was purged by H_2 and pressurized to 6 MPa at room temperature, and the inlets and outlets were shut. Hydrogenolysis took place by soaking the reactor at 450 ℃ for 1 h at 100 rpm. After hydrogenolysis, the reactor was cooled down to room temperature. All the gases were vented without characterization. All solid and liquid products were transferred into a beaker. The reactor head vessel was rinsed by THF. All the rinsing THF was transferred into the beaker as well. The product-THF mixture was filtered through a quantitative ashless Grade 42 filter paper (Whatman®, 1.5 μm pore size) in a Büchner funnel. The filter cake was dried in a drying oven at 105 °C for 24 hours, and collected as THF-insoluble. The filtrate was vacuum-dried at 60 °C to remove THF, collected as PDL (THF-soluble).

2 Mild solvolysis liquefaction procedure

The mild solvolysis liquefaction to acquire coal-plastic liquid was also conducted in the setup of HDPE hydrogenolysis. Dry coal powder and PDL were mixed by mass ratio of 1:1 (160 g vs. 160 g), and stirred by a glass rod to get slurry. The slurry was loaded into the vessel of the reactor, and the vessel was assembled. The subsequent operations were the same as HDPE hydrogenolysis. The reactor was soaked at 400 ℃ for 1 h at 100 rpm under initial H_2 pressure of 6 MPa. After collecting product and rinsing the reactor and vessel by THF, the product was filtered, and the filtrate was distilled at 105 ℃ under N_2 to remove THF and water to get THF-soluble fraction. The product further underwent Soxhlet extraction to remove hexane-soluble fraction. The colleccted product was THF-soluble and hexane-insoluble, called coal-plastic liquid.

3 Thermal upgrading of coal-plastic liquid

Thermal upgrading of coal-plastic liquid was conducted in a custom-designed 316 stainless steel stirring reactor (capacity 739.34 mL), heated by a sand bath heating system. Coal-plastic liquid was fed into the reactor and thermally treated at different temperatures and soaking times (will be discussed in Results and discussion) under continuous N2 flow. The stirrer maintained 100 RPM. After the soaking time, the reactor was cooled under N_2 gas flow. The residue in the reactor was collected as mesophase coal-plastic liquid (MCPL).

4 Characterization of coal-plastic liquid and MCPL[1]

4.1 Quinoline insoluble

The quinoline insoluble content was determined according to ASTM D2318-20 (ASTM 2020). In short, a sample was thoroughly dissolved in quinoline and the sample-quinoline mixture was filtered. Quinoline insoluble was calculated as the weight of dried filter cake divide by weight of sample.

4.2 Nuclear Magnetic Resonance

A 1H NMR analysis was performed on a 500 MHz 1H NMR spectrometer (AVANCE III HD, Bruker, Billerica, MA, USA). Each tar sample was dissolved in deuterochloroform (CDCl3) with 1 vol% tetramethylsilane (TMS) as an internal reference. Proton chemical shifts were assigned to the following categories: H_{ar} represents the percentage of protons in aromatic structures (chemical shift at 8.5 to 6.6 ppm). H_{α} represents the percentage of protons near the carbon atom in the α-position of aliphatic substituents of aromatic structures (chemical shift at 4.0 to 2.2 ppm). H_{β} represents the percentage of protons in methylene groups (chemical shift at 2.1 to 1.1 ppm). H_{γ} represents the percentage of protons in the terminal methyl groups of the alkyl moieties of molecules (chemical shift at 1.1 to 0.3 ppm). These structural proton fractions were used to assess solvent reactivity and potential hydrogen-donating behavior. All the spectra were acquired at 25 °C with a 64-scan average.

4.3 Mesophase content

Mesophase textures were examined using a polarized light microscope (BH200-MR, Ningbo Sunny Instruments Co., Ltd., Ningbo, China), equipped with a polarizer, wave retarder, and oil-immersion objectives. Samples were embedded in epoxy resin and polished sequentially with silicon carbide papers (360, 600, 800, 1200 grit), followed by a 2 min polish with a 1 μm diamond suspension (Buehler MetaDi). Images were taken at 10× magnification under crossed polarizers. For each sample, 12 images from different fields were analyzed. The mesophase content was quantified based on modified ASTM D4616-95 (2018) method using an image analysis tool developed in a previous work.[2] In short, the quantity of pixels of bright area on the image divide by the quantity of pixels belonging to the sample is the mesopahse content. The results were averaged over all the images.

4.4 Softening point

The softening points of the mesophase pitch samples were measured using a hybrid rheometer/DMA (HR 20, TA Instruments, New Castle, DE, USA) under a nitrogen atmosphere. The samples were formed into 1/8-inch diameter disc and loaded under parallel plate geometry with 0.2 N compression. After the sample was equilibrated at 35 °C, the temperature ramped at 5 °C/min to 400 °C. The curve disc placement vs. temperature was recorded. On temperature derivative of displacement, the temperature at the peak is the softening point.[2] Each sample was tested twice; the values reported are the averages.

5 Supplementary results

5.1 Utah Sufco coal

Table S1 Proximate and ultimate analysis of Utah Sufco coal.*

Ash	C	H	N	S	O	H_2O	Volatiles
8.9	79.4	5.6	1.3	0.4	13.3	6.1	41.0

*: Cited from Wang et al[1]

5.2 PDL

The yield of PDL from HDPE hydrogenolysis was 21.5 ± 3.3%. On 1H-NMR spectra, hydrogens of PDL were categorized based on their chemical environments indicated by chemical shifts. Four categories, H_{ar}, H_{α}, H_{β} and H_{γ}, were identified, and their contents were quanfitied by percentages of peak area, shown in Table S2. The contents are 21.1%, 35.8%, 27.7%, and 15.4%, respectively. Tetralin has H_{ar}, H_{α}, and H_{β}, their contents are all 33.3%. The categories of hydrogens was corroborated by published non-catalytic hydrogenolysis results[3,4] whose liquid products included aliphatics (alkanes, cycloalkanes, and olefin), and aromatics. HDPE has no aromatics, but PDL contained H_{ar}. Since no catalysts were used in our process, aromatics were possibly formed through a thermal radical route. When heated, random scission breaks HDPE into long-chain radicals. Radicals experience β-scission, cyclization, hydrogen abstraction, and recombination.[5,6] If cyclization takes place, a radical coils and reacts with itself.[6] This cycloalkane is dehydrogenolyzed and forms an aromatic ring. As the reaction progresses, monoaromatics can condensate into polyaromatic hydrocarbons such as naphthalene. However, we cannot determine a dominant pathway without more experiments and characterizations. This is beyond the scope of this study. Unlike pyrolysis, the molecular-hydrogen-saturated radicals inhibited coking and repolymerization.[5] This work also compared the coal-plastic liquids produced by both tetralin and PDL as the solvents. The H_{ar} contents were 60.93% and 70.5%, and the yields were 63.4 ± 0.9% and 62.1 ± 4.3%, respectively. Tetarlin led to lower H_{ar} content and slightly higher yield, suggesting tetralin had a stronger hydrogenation effect, which added more hydrogen to aromatics and assisted bond breaking of the coal. The stronger hydrogenation effect was because all THN molecules were donors, while PDL was a mixture of donors and non-donors.

Table S2 1H-NMR results of PDL and THN.*

	H_{ar}	H_{α}	H_{β}	H_{γ}
PDL	21.1	35.8	27.7	15.4
THN	33.3	33.3	33.3	0

*: Cited from Wang, et al[1]

H_{ar}, H_{α}, H_{β} and H_{γ} were identified. H_{ar} indicates hydrogen on aromatic rings, H_{α} is hydrogen on carbon α to aromatic ring, H_{β} is hydrogen on methylene and methylidyne groups. H_{γ} belongs to the methyl group.[7,8]

5.3 MCPL

Elemental analysis of MCPLs is shown in Table S3. The sum of the weight percentages was not 100% because there was a ±2% error in the carbon values, as indicated by the instrument manager. The distributions of MCPLs were similar. Carbon content is over 90%, and hydrogen is between 3.71% and 3.98%. The oxygen content is slightly higher than 2%, and nitrogen and sulfur account for less than 1%. As shown in the MCPL properties in Table 1 and the m/z distribution in Fig. 3, from MCPL1 to MCPL3, an increasing softening point, quinoline insolubility, mesophase content, and average m/z value indicate more thorough thermal upgrading. MCPLs should thus experience more condensation and elimination of heteroatoms. However, elemental analysis of Table 2 showed carbon content did not follow this trend. This was possibly because the increase of carbon content was low and was muted by the ±2% error.

Table S3 Elemental analysis of MCPLs.

Sample	C	H	N	O	S	Sum
MCPL1	91.41%	3.98%	0.87%	2.02%	0.37%	98.65%

Sample	C	H	N	O	S	Sum
MCPL2	92.65%	3.71%	0.85%	2.22%	0.29%	99.72%
MCPL3	92.00%	3.97%	0.89%	2.08%	0.28%	99.22%

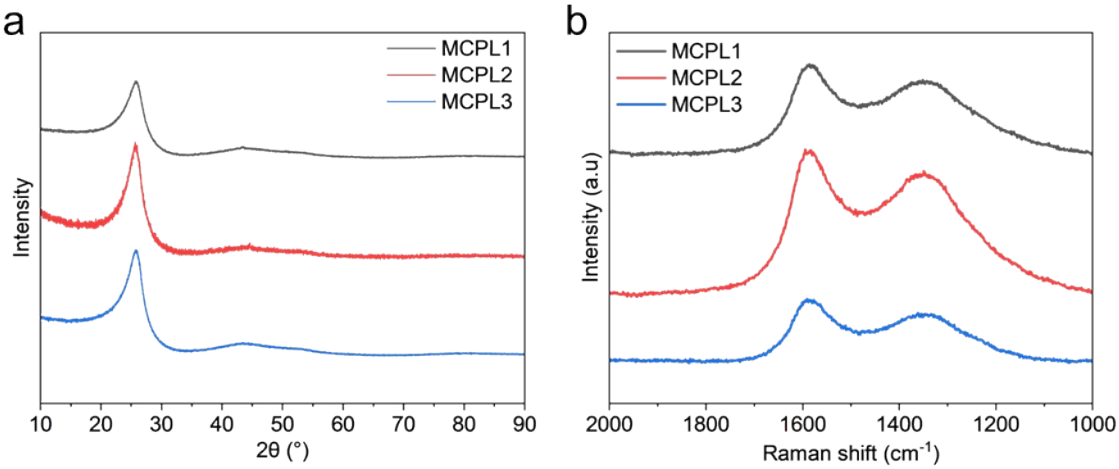

Fig. S1 Crystalline curves of MCPLs. (a) XRD pattern, (b) Raman spectra.

Table S4 Crystalline data from XRD pattern and Raman spectra of MCPL extracted from Fig. S1.

Sample	Condition	$2\theta_{002}$ (°)	FWHM (°)	d_{002} (nm)	L_c (nm)	N	I_D/I_G	L_a (nm)
MCPL1	380 °C, 6 h	25.80	2.82	0.3449	3.09	9.97	0.84	5.21
MCPL2	410 °C, 3 h	25.68	2.51	0.3465	3.47	11.02	0.85	5.15
MCPL3	425 °C, 3 h	25.76	2.83	0.3454	3.08	9.92	0.78	5.62

Polarized micrographs of MCPL are shown in Fig. S2.[1] MCPL1 (Fig. S2a) shows anisotropic optical textures with small mesophase domains (bright dots) indicated by yellow arrows. However, an upgrading temperature of 380 °C was still insufficient for forming significant mesophase regions. At a higher temperature of 410 °C, larger, more coalesced mesophase regions appeared on MCPL2, please see yellow arrows in Fig. S2b. As the upgrading temperature was increased to 425 °C (Fig. S2c and S2d), MCPL3 exhibited an ideal mesophase optical texture, with the entire pitch surfaces covered by large lamellar mesophase domains exceeding 100 μm in size.

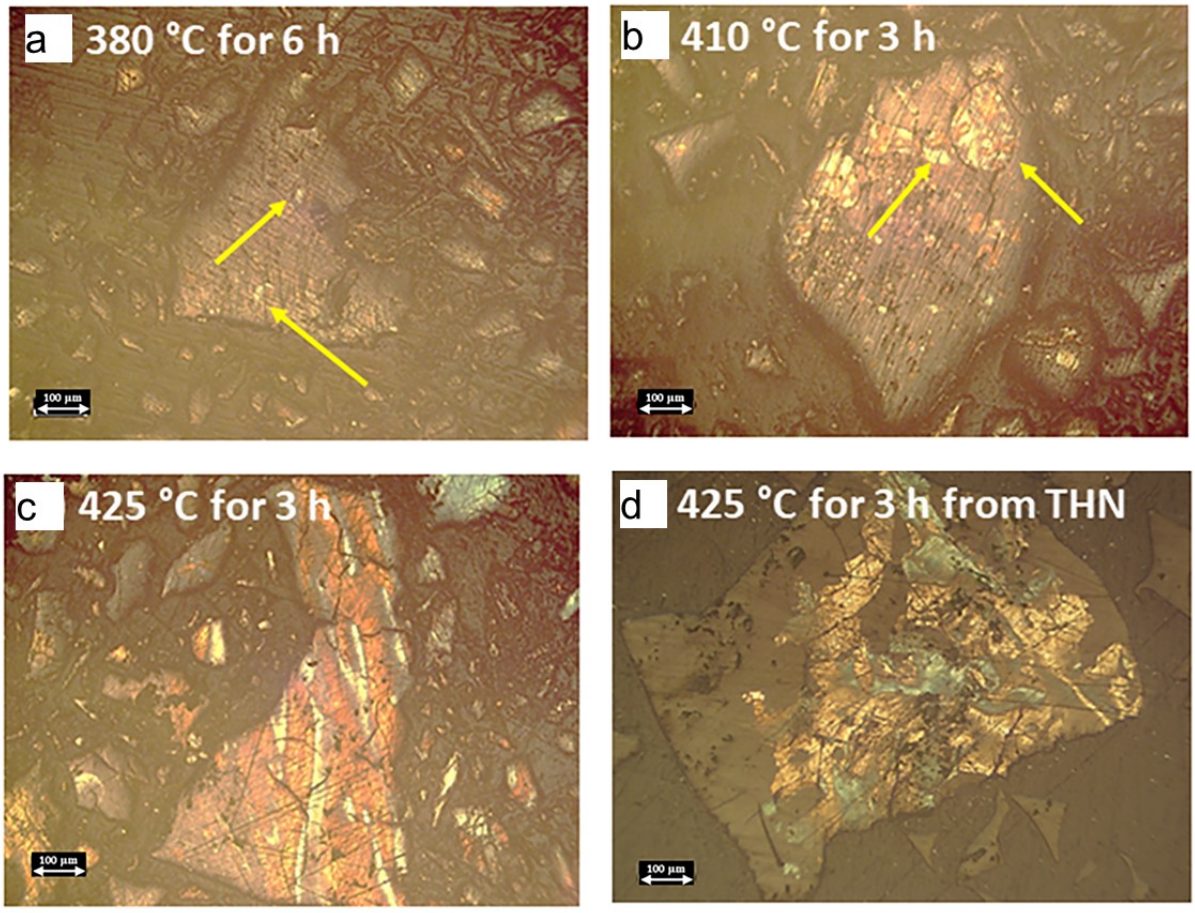

Fig. S2 Polarized micrographs of MCPLs treated at different conditions. (a) MCPL1, (b) MCPL2, (c) MCPL3, and (d) MCPL3-THN. (a), (b), (c), and (d) in are cited from (c), (e), (h), and (i) of Figure 3 in Wang et al,[1] respectively.

5.4 CFs

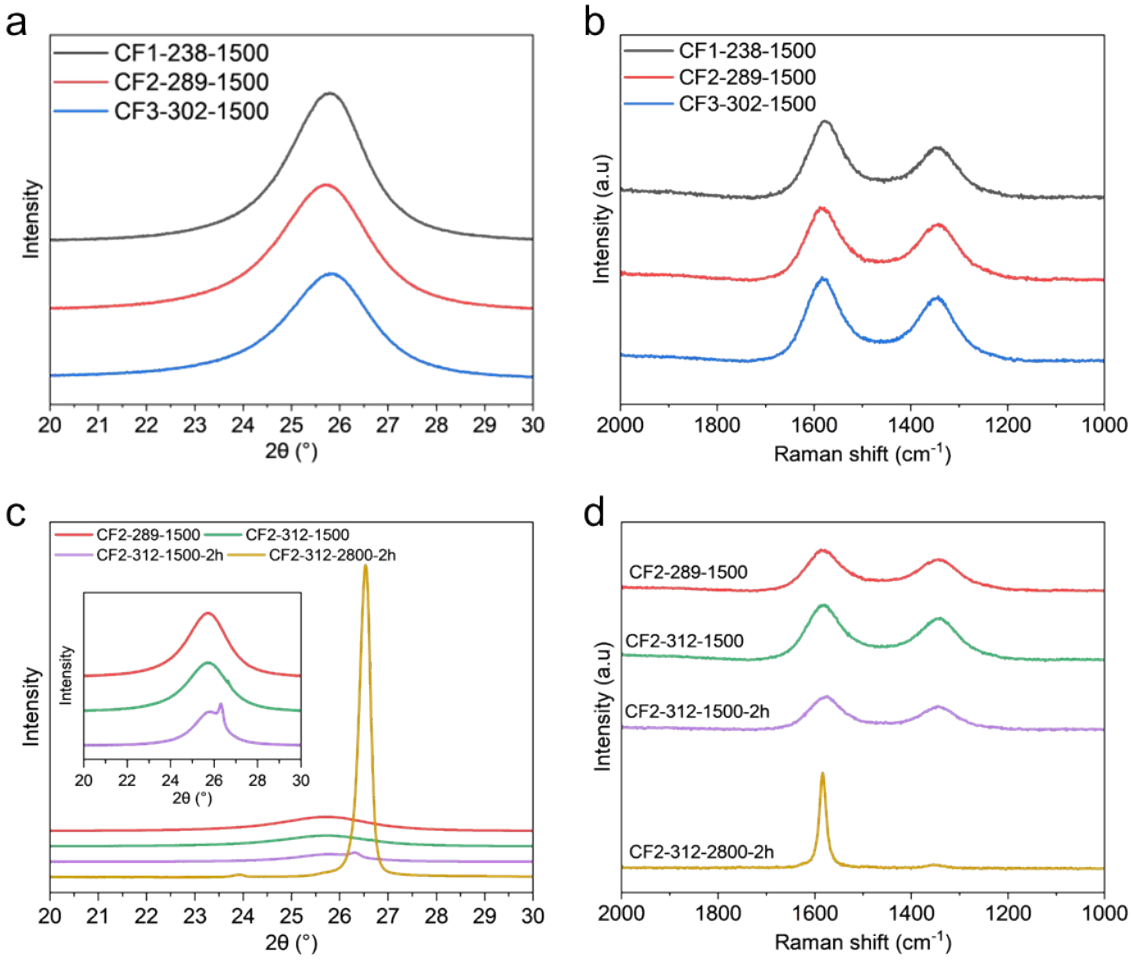

Fig. S3 Crystalline curves of CFs. (a) and (c): XRD pattern; (b) and (d): Raman spectra.

Table S5 Crystalline data from XRD pattern and Raman spectra extracted from Fig. S3.

Sample	$2\theta_{002}$ (°)	FWHM (°)	d_{002} (nm)	L_c (nm)	N	I_D/I_G	L_a (nm)
CF1-238-1500	25.79	1.83	0.3450	4.77	14.81	0.66	6.64
CF2-289-1500	25.70	2.11	0.3462	4.13	12.93	0.78	5.68
CF3-302-1500	25.79	1.99	0.3450	4.38	13.70	0.78	5.66
CF2-312-1500	25.67	2.10	0.3466	4.15	12.97	0.77	5.75
CF2-312-1500-2h	26.31	1.36	0.3383	6.44	20.04	0.70	6.31
CF2-312-2800-2h	26.53	0.26	0.3356	33.76	101.60	0.05	83.44

Table S6 Mechanical test results of different CFs made from different MCPLs.

CF	n	d (um)	YM (GPa)	TS (GPa)	ε (%)
CF1-238-1500	24	45.8 ± 3.1	75 ± 17	0.54 ± 0.14	0.80 ± 0.29
CF2-289-1500	15	10.8 ± 1.9	194 ± 38	0.85 ± 0.39	0.47 ± 0.17
CF3-302-1500	17	28.7 ± 2.7	135 ± 26	0.68 ± 0.18	0.54 ± 0.11

CF	n	d (um)	YM (GPa)	TS (GPa)	ε (%)
CF2-266-1500	13	10.2 ± 2.2	169 ± 32	0.81 ± 0.21	0.54 ± 0.14
CF2-312-1500	14	11.5 ± 2.4	201 ± 30	1.11 ± 0.18	0.63 ± 0.09
CF2-335-1500	13	12.0 ± 1.7	173 ± 26	1.08 ± 0.15	0.64 ± 0.11
CF2-312-1500-2h	11	11.7 ± 2.0	238 ± 37	1.15 ± 0.22	0.52 ± 0.10
CF2-312-2800-2h	15	8.2 ± 1.8	759 ± 71	4.03 ± 0.76	0.59 ± 0.13

The number before "±" is the average, and the one after is the standard deviation; "2h" means carbonized for 120 min, a CF without "2h" means carbonized for 10 min. "n" is the quantity of filaments tested.

Table S7 Weight change of CFs during treatment.

CFs	Stabilization gain	Yield
CF1-238-1500	5.67%	86.08%
CF2-289-1500	6.90%	89.39%
CF3-302-1500	-7.06%	74.12%
CF2-266-1500	10.53%	52.63%
CF2-312-1500	2.90%	91.30%
CF2-335-1500	-17.14%	74.29%
CF2-312-1500-2h	2.90%	77.39%
CF2-312-2800-2h	2.90%	70.74%

$$Stabilization\ gain = \frac{Wt\ of\ FCFs\ after\ stabilization - Wt\ of\ FCFs}{Wt\ of\ FCFs} \times 100\%$$

$$Yield = \frac{Wt\ of\ FCFs\ after\ carbonization\ or\ graphitization}{Wt\ of\ FCFs} \times 100\%$$

References

1 W. Wang, A. Gallacher, K. Jolley, M. G. Nelson and E. Eddings, Harnessing high-density-polyethylene-derived liquid as a model solvent for the co-liquefaction of low-rank coals: toward sustainable mesophase pitch for making high-quality carbon fibers from waste plastics, *Sustainability*, 2025, **17**, 4750.

2 J. Malzahn, I. Preciado, D. Wang, M. Weisenberger and E. Eddings, Effect of secondary gas-phase reactions (SGR) in pyrolysis of carbon feedstocks for anisotropic carbon materials production – 1: Controlling SGR to modify intermediate coal tar species to improve pitch anisotropy, *J Anal Appl Pyrolysis*, 2022, **164**, 105541.

3 I. HAKKIMETECAN, A. OZKAN, R. ISLER, J. YANIK, M. SAGLAM and M. YUKSEL, Naphtha derived from polyolefins, *Fuel*, 2005, **84**, 619–628.

4 W. Ding, J. Liang and L. L. Anderson, Thermal and catalytic degradation of high density polyethylene and commingled post-consumer plastic waste, *Fuel Processing Technology*, 1997, **51**, 47–62.

5 D. Munir, M. F. Irfan and M. R. Usman, Hydrocracking of virgin and waste plastics: A detailed review, *Renewable and Sustainable Energy Reviews*, 2018, **90**, 490–515.

6 A. Kossiakoff and F. O. Rice, Thermal Decomposition of Hydrocarbons, Resonance Stabilization and Isomerization of Free Radicals [1], *J Am Chem Soc*, 1943, **65**, 590–595.

7 D. Fang, G. Wang, Q. Sheng, S. Ge, C. Gao and J. Gao, Preparation of hydrogen donor solvent for asphaltenes efficient liquid-phase conversion via heavy cycle oil selective hydrogenation, *Fuel*, 2019, **257**, 115886.

8 M. D. Guillén, C. Díaz and C. G. Blanco, Characterization of coal tar pitches with different softening points by NMR, *Fuel Processing Technology*, 1998, **58**, 1–15.